



# The effect of pre-heat temperature on the formability of a glass-fibre/polypropylene and steel-based fibre–metal laminate

Davood Rahiminejad<sup>1</sup> · Paul Compston<sup>1</sup>

Received: 2 February 2020 / Accepted: 28 April 2020 / Published online: 9 May 2020  
© Springer-Verlag France SAS, part of Springer Nature 2020

## Abstract

This paper presents an experimental and numerical investigation into the effect of pre-heat temperature on stretch forming of a fibre metal laminate (FML) comprised of alternating layers of steel and woven (0/90) glass-fibre polypropylene in a 2:1 configuration. Hourglass sample geometries were formed in an open die and real-time photogrammetry was used to measure the evolution of strain fields over the lower surface of each sample. The sample pre-heat temperatures were 140 °C (above the crystallization temperature) and 170 °C (melt temperature of polypropylene). For each temperature, a forming limit curve (FLC) was determined based on ISO 12004-2:2008 and compared to the FLC of the steel skin. The experimental results demonstrate that pre-heat temperature of 140 °C enables sufficient matrix flow such that the formability of the FML is comparable to the formability of the steel sheet. Furthermore, the FML stretch-forming process was simulated using commercial finite element software, LSDYNA, with an explicit solver. The glass-fibre polypropylene material behaviour was simulated with a curve fitting technique of material characterization test results. A user-defined subroutine (UMAT) was developed for the composite material modelling through all process temperatures. The simulation, justified with experiments, provided a numerical model of the hybrid material to utilise for forming complex shapes.

**Keywords** Fibre–metal laminate · Temperature · Forming limit curve · 3D photogrammetry

## Introduction

Fibre metal laminates (FMLs) are comprised of alternating thin layers of metal and fibre reinforced polymer composite. They are designed to take advantage of the high specific strength and stiffness properties [1] and fatigue resistance of composites [2], and the toughness of metals [3]. FMLs also exhibit excellent impact perforation resistance compared to metals [4]. In particular they are a light-weight alternative to monolithic sheet metal and one of the most notable applications is an FML based on aluminium and glass-fibre/epoxy (GLARE) in the fuselage of the Airbus A380 [5].

A major obstacle to further adoption of FMLs based on thermoset polymers such as epoxy is the relatively time-consuming manufacturing process compared to monolithic metal forming. The placement of the composite layers is not

conducive to automated processes and thermoset resins required cure cycles in the order of hours. Alternatively, FMLs with a thermoplastic composite layer offer the potential for rapid production as the polymer can be heated to a softening or melting temperature, then formed and cooled in the order of seconds in a one-shot stamp forming process. Thermoplastics also offer the potential for recyclability.

Stamp forming is a well-known rapid production technique for metallic part production in many industries. The forming limit diagram (FLD), developed by Keeler and Backhofen [6], is an in-plane principal strain space diagram that is utilised for evaluating sheet metal formability. A major aspect of an FLD is a forming limit curve (FLC), which separates the safe region from failure area in the principal strains space. The FLC is determined at the onset of the localised necking at different deformation modes, as a ratio of minor to major strains. The Nakazima test [7] and Marciniak in-plane test [8] are the two standard procedures for determining the FLC as described in ISO 12004-2 [9]. In the Nakazima test method, stretch forming to failure is carried out on samples with different middle widths from narrow to full circular with a hemispherical punch. Although this approach was originally developed

✉ Davood Rahiminejad  
Davood.rahiminejad@anu.edu.au

<sup>1</sup> Research School of Engineering, Australian National University, Canberra 2601, Australia

for monolithic metals, it has been adopted to investigate formability of FMLs and sandwich structures [10].

Therefore, there is a great potential to rapidly stamp-form FMLs with thermoplastic composite layer and much research has been undertaken to understand the effect of forming process parameters. Mosse et al. [11] demonstrated increasing feed rate reduces shape error and delamination in the FMLs in channel forming. Mosse et al. [12] also showed pre-heat temperature, squeezing force and shear displacement rate play an important role in transferring the interfacial load between FML layers. Gresham et al. [13] investigated the effects of blank-holder forces and pre-heat temperature on the dome forming of FMLs with glass-fibre-reinforced polypropylene (GFPP) composite layers and demonstrated that blanks experienced tear and fracture under higher blank-holder forces, and wrinkle under lower blank-holder forces. It was also shown an increase in pre-heat temperature led to a decrease in the core composite failure.

Further evidence of the potential for forming of polypropylene-based materials is provided by work with FMLs based on self-reinforced polypropylene (PP). Mosse et al. [14] showed reduced spring-back after channel forming of a pre-heated (160 °C) aluminium/self-reinforced PP FML compared to monolithic aluminium; and for the same channel-formed FML, Compston et al. [15] showed lower major strain at sidewalls compared to aluminium. Sexton et al. [16] studied the stretch forming of self-reinforced PP FMLs with aluminium substrates and concluded that the FML is comparable to plain aluminium in terms of the forming limit curve (FLC), and also showed that FML experienced higher allowable major strain before failure. Deep-drawing of thermoplastic metal composites were investigated numerically and experimentally under different blank-holder forces and temperatures by Rajabi et al. [17]. It was concluded increasing temperature of the blanks led to a reduction in the blank-holder forces. The FMLs utilising both glass-fibre and self-reinforced composites were formed normally under higher blank-holder forces at 150 °C temperature. Wollmann et al. [18] investigated, numerically and experimentally, the stiffness properties and the deep cup drawing process of FMLs made of steel sheets and carbon fibre-reinforced thermoplastic. They showed that deep cup drawing of the FMLs was possible to some extent. The dominant failure modes of the FML during the cup forming process were cracking and wrinkling of the steel sheets and fibre failure in the composite material. The formability of FMLs was investigated by experimental and numerical methods based on the M–K (Marciniak–Kuczynski) theory by Aghchai and Khatami [19]. The FMLs are comprised of aluminium and chopped glass-fibre reinforced polypropylene sheets. Uniaxial tensile and stretch-forming tests were conducted to determine

the forming limit diagram (FLD), and consequently the FLC. The numerical model predicted necking strains to within 9% of the experimental data. It was also concluded that increasing the thickness of the composite core as well as the overall FML thickness significantly improved the average formability.

While much research has been directed at the formability of aluminium-based FMLs, the formability of steel-based FMLs is less well understood. A material system comprised of the steel layers and a glass fibre reinforced thermoplastic composite offers interesting characteristics of lower density and cost and higher impact resistance. Stamp-forming provides an opportunity to utilise this material system for industrial applications, however it requires identifying the optimum process parameters for forming steel-based FMLs up to a reasonable range. This paper therefore presents a study of the effect of pre-heat temperature, one of the key processing parameters, on the formability of a glass-fibre PP and steel-based FML with interlayer FML investigation through the process. The interlayer interaction of this hybrid system during forming is taken into consideration. Unlike the pre-heated FMLs, the glass fibre reinforced PP FMLs at room temperature have exhibited poor forming characteristics. Reyes and Kang [2] showed a fibre-glass reinforced PP aluminium-based FML at room temperature is able to experience 7% major strain in the plane strain mode at the safe region. Considering the total elongation of the steel sheet in uniaxial extension is around 40%, forming glass-fibre PP and steel-based FMLs at room temperature leads to deteriorating steel formability due to the failure of the glass-fibre PP composite in the early depth of forming. Hence, the pre-consolidated FML hourglass-shaped samples, known as blanks, were formed to failure in the stretch forming conditions at the pre-heat temperatures of 140 °C, just above the PP crystallization temperature, and 170 °C, PP melting temperature [12, 20]. Then, forming limit curves (FLCs) were determined using an ARAMIS system and compared to the FLC of the steel sheet. The strain path evolutions of the induced deformation modes, up to the blank failure, were used to elucidate the FML formability. To study the process numerically, a finite element (FE) simulation of the FML stretch-forming process was conducted with LSDYNA commercial software, an explicit solver. It also has a capability of implementing the FLCs, obtained from the experiments, into the FE model. FML constituents' material characterization tests were carried out based on the relevant standards. The composite material behaviour was simulated using a user-defined curve and the composite modelling was developed with a user-defined subroutine (UMAT) and the steel was simulated using built-in material modelling of LSDYNA.

## Experimental procedure

### Materials and laminate production

The fibre metal laminates (FMLs) were comprised of 0.45 mm thickness hot-dipped zinc-coated sheet steel (BlueScope Limited) and a 0/90 twill weave fibre-glass reinforced polypropylene (GFPP) (Owens Corning, Twintex®) of 60% fibre weight fraction, 1485 g/m<sup>2</sup> ply weight and 1 mm thickness. A modified polyolefin hot-melting adhesive (Collano® 22.010) with a minimum bonding temperature of 130 °C and a density of 0.9 g/cm<sup>3</sup> was used to bond the steel and GFPP. The FMLs were produced using a compression moulding process. Alternate layers of steel and composite, in a 2:1 configuration shown in Fig. 1, and with a layer of the adhesive at each steel-composite interface were heated to 170 °C in a platen press. These layers were then consolidated at a pressure of 400 KPa for two minutes to assure uniform bonding quality over the sample area then rapidly water cooled.

### Material characterization

Uniaxial tensile tests were conducted on the steel cut into a dog-bone shape at rolling, 45 degree, and transverse directions to the sheet rolling direction according to ASTM A370. Furthermore, material properties of The GFPP were investigated at different ambient temperatures from room temperature to 170 °C (the composite matrix melting temperature). The GFPP test samples were prepared in a rectangular shape with 25 mm width and 250 mm length cut from 1 mm pre-consolidated sheets based on ASTM D3039, with 0/90 and ± 45° fibre orientations to the GFPP fibre directions (weft and warp). 50 mm long aluminium tabs were bonded to the GFPP specimens to avoid premature failure in the testing machine grips. A water jet cutter was used to prepare all samples. Tensile tests were conducted at a crosshead displacement rate of 5 mm/min in an Instron™ 8874 universal testing machine,

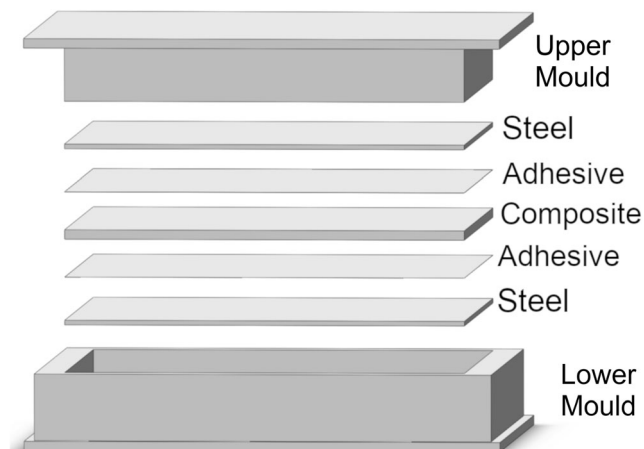


Fig. 1 FML layup configuration

equipped with a heat chamber. The full field strain for each sample during testing was measured using a real-time photogrammetry system (ARAMIS). The Material characterization test setup is shown in Fig. 2.

### Forming specimen geometry

ISO 12004-2 recommends several specimen geometries for stretch forming tests from which the hourglass shaped samples were selected for this study. The FMLs were cut into hourglass shaped specimens with 25, 50, 75, 100 mm middle widths, and a full circular one with 200 mm diameter (Fig. 3) using a water jet cutter.

### Forming tests

A custom-built 30 t hydraulic press machine with an open die 105 mm in diameter, and a 100 mm hemispherical punch, was used to perform the stretch-forming experiments. Forming in an open die was necessary to enable measurement of the strain field evolution over the bottom surface of blanks in real time during the forming process using real-time photogrammetry. The pre-heat temperatures for the FMLs were 140 and 170 °C. The stretch forming was also conducted on the monolithic steel sheet with 0.45 mm thickness.

A local PC control system was used to set process parameters, including punch feed rate and punch displacement. Experiments were carried out up to failure point defined by a punch load drop of 20%. ISO 12004-2 recommends forming metallic blanks at 1.5 mm/s to generate a FLC, while several

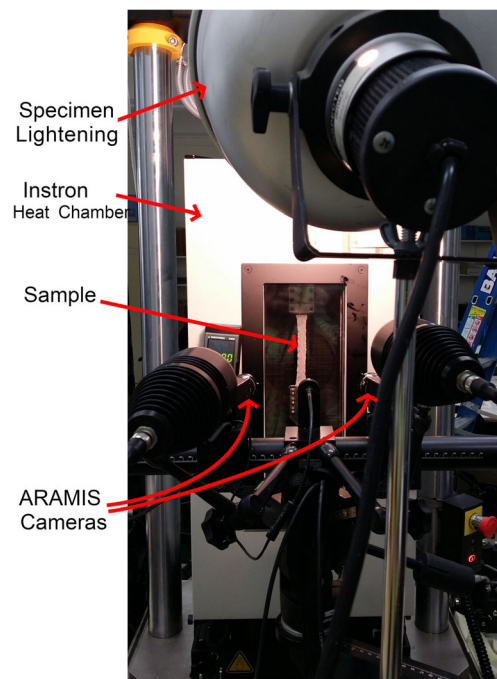
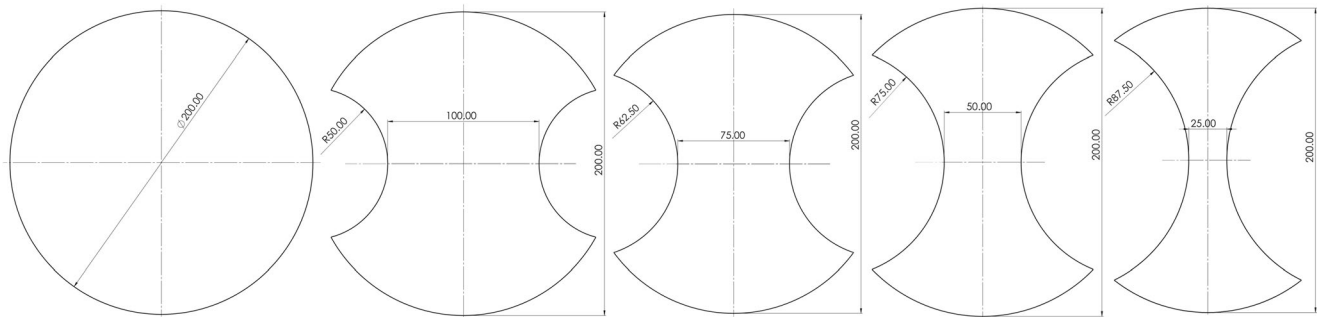


Fig. 2 Material characterization test setup



**Fig. 3** Hourglass shaped geometries

studies on the forming of pre-heated fibre-reinforced composites suggested that a higher feed rate is optimum. Hou and Friedrich used a feed rate of 4.2 mm/s to form pre-consolidated PP matrix composite at high temperature with a blank-holder closing rate of 70–230 mm/s [21]. MacHado et al. stated that a low feed rate affected the mechanical properties, especially shear behaviour, of composites during high temperature forming, and hence the isothermal assumption becomes invalid [22]. Tepex® Dynalite, a manufacturer of glass PP consolidated laminate, recommended a feed rate of 50 mm/s up to 10 mm before the ultimate forming depth and then 5 mm/s up to the end of the process [23]. In this study, a feed rate of 10 mm/s was chosen to perform the stretch-forming tests [16].

A blank holder and die were used to apply a stretching condition over samples during the forming process which are imposing fixed boundary conditions over the sample peripheral region and leading samples experiencing failure at their centre. Therefore, the blank-holder force had to be sufficient to apply fixed constraints on FMLs and while avoiding any premature failure at the lock ring, or blank slippage into the die during the forming process. In this case, 60 N m torque on the lock ring bolts (twelve M12 bolts) ensured stretch forming conditions and no evidence of premature failure at the lock ring was observed.

Prior to forming, the FML samples mounted on the portable lock ring were pre-heated in a convection heat chamber. The average time required for samples to be reached to the test temperature was 2 h. Thermocouple and infrared thermometer were used to measure the sample temperature. The uniformity of temperature over the sample was checked through embedding 3 thermocouples in 3 different locations of the sample. After the sample was reached the target temperature, they were transferred into the press machine in less than 5 s and immediately stamp formed.

A schematic of the forming setup including the press machine, the blank, the blank holder and die, and the photogrammetry system is shown in Fig. 4. The full field strain for each sample during the forming process was measured directly using a real-time photogrammetry (ARAMIS by GOM mbH). This system is comprised of two high-speed, CCD

cameras to take images, and develops a three-dimensional measurement field from correlation of two images. The cameras had 5 megapixel resolution and 17 mm focal lens. Cameras were calibrated to provide deformation depth of 180 mm to cover sample deformation completely. Spray painting of stochastic patterns of black dots on white background, a pixel is assigned to each dot whose displacement is measured and computed into full strain field over the surface captured with cameras [24]. Subset size was 19 pixels to perform analyse.

Figure 5 shows a schematic diagram of how an FLC is generated. A strain ratio,  $\beta$ , whose limit strains at the onset of necking determines the FLC, is induced on the blanks, depending on the geometry of the blank and friction between the hemispherical punch and the blank during stretch-forming. Stretch forming of geometries with various middle widths imposes different principal strain states over blanks. Generally to cover two dimensional principal strain states, stretch forming of hourglass shaped samples ranging from 25 to 100 mm middle width and full circular samples are required. Hourglass-shaped blanks with middle widths less than 100 mm experience negative strain ratios. Forming an hourglass shaped sample of 100 mm width leads to a plane strain deformation with  $\beta = 0$ , whereas a full circular blank

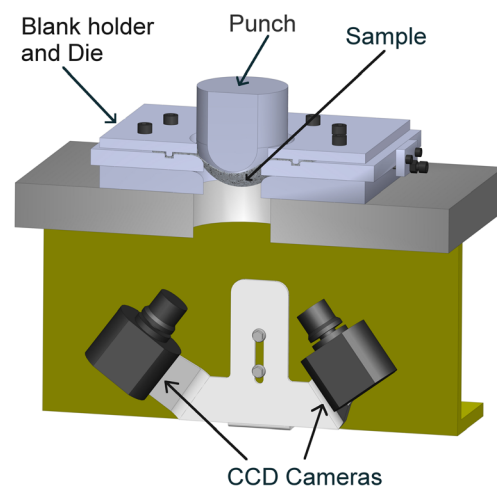


**Fig. 4** Schematic of stamp forming experimental setup

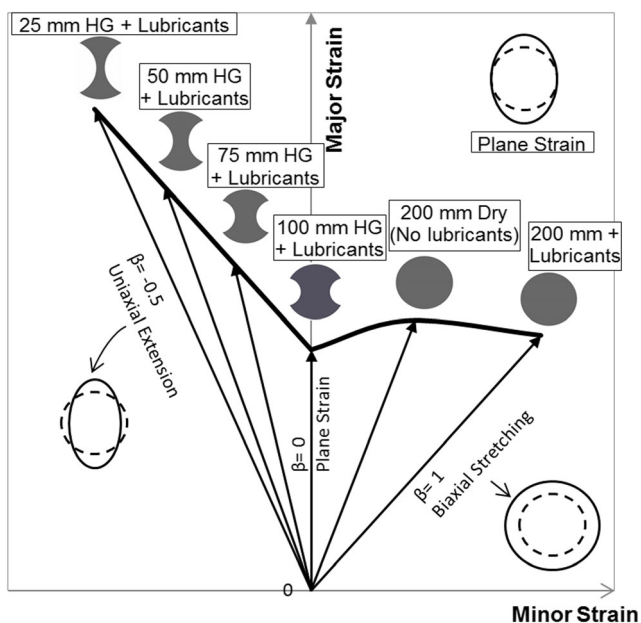


**Fig. 5** Deformation modes are imposed on a blank based on blank shapes on the forming limit diagram to establish a FLC

under the stretching condition leads to a biaxial stretching mode with  $\beta = 1$ . To impose these strain ratios and hence strain paths, the friction state has to be close to zero and this is achieved by applying lubricants like Vaseline and Teflon together. However, to impose a deformation mode with a strain ratio between the plane strain and biaxial stretching modes demonstrated in Fig. 5, it is necessary to perform stretch-forming on a full circular blank without any lubricants between the punch and the blank (a ‘dry’ condition) [25]. This deformation mode was just applied to the steel, resulting in the stretch-forming of a full circular steel blank without any lubricants.

$$\beta = \frac{\text{Minor Strain}}{\text{Major Strain}} \quad (1)$$

### Forming limit curve (FLC) determination

The FLC of steel was determined using the Nakazima test method and the FLC mode of ARAMIS based on ISO 12004-2. According to this method, blanks with five different geometries from narrow middle widths to full circular were formed to failure using a hemispherical punch. The limit strains at the onset of necking for each deformation mode were calculated and the FLC determined. The strain tensor method for measuring a strain field over the blanks was hencky (logarithmic) strain tensor. For example, the limit strains for a 25 mm hourglass-shaped steel specimen were determined as follows. Figure 6a shows the major strain field at the image acquired immediately prior to cracking. Three sections were

drawn 2 mm apart, parallel to each other and perpendicular to the crack that appeared in the next image (Fig. 6a); major and minor strain graphs were then extracted for each section (Fig. 6b). These graphs were curve-fitted using a parabolic function based on the ISO 12004-2 standard. The extrema of the fitted curves were determined and their averages were taken to be the limit strains at the onset of the necking for the imposed deformation mode.

## Results and discussions

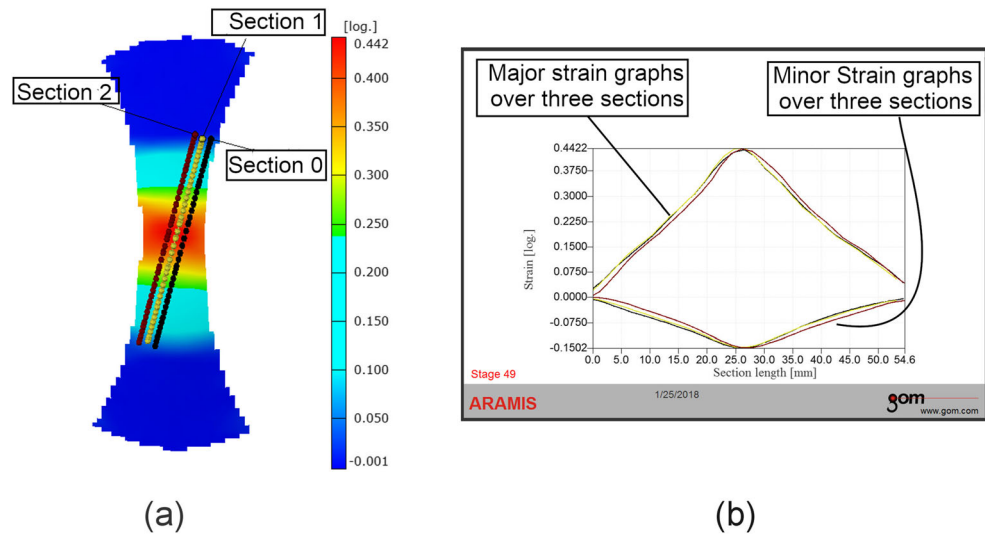
### Steel tensile properties

The two sample engineering stress-strain graphs (specified with the sample number in the legend) of the steel at each rolling, 45°, and transverse directions are shown in Fig. 7. The anisotropic behaviour of the steel is mostly observed in the region immediately beyond the elastic area of the curve, which extends up to the point of 13% strain. After that, the steel shows a similar plastic behaviour in all directions up to the point of failure. To acquire the initial yield point of the steel sheet, an extensometer was embedded to the steel sample during uniaxial extension experiment to measure strain-stress curve precisely. The test results showed a distinctive point between linear elastic region and plastic region which led to determination of the initial yield point of the steel sheet. The acquired yield point is in accordance with the steel yield point specified in data sheet of the steel sheet provided by the manufacturer, BlueScope Limited. Overall, the steel shows an average initial yielding point of 365 MPa, modulus of elasticity of 210 MPa and average total elongation of 40%, with 10% variation in the specimens.

### The GFPP tensile material properties

The engineering stress-strain graphs of the GFPP with 0/90 fibre orientation (warp and weft) at different ambient temperatures are shown in Fig. 8. The GFPP at room temperature has a strain at failure of 2.8% at almost 190 MPa. The GFPP at higher temperatures show an increase in the GFPP strain at failure and also strength, since the GFPP matrix softens or melts down. The GFPP at 100 °C demonstrates a linear mechanical behaviour up to failure at 4.3% strain and 195 MPa stress. Performing a GFPP uniaxial extension test at 120 °C results in decreasing the GFPP modulus of elasticity and increasing the material strength to 200 MPa and 5.25% strain at failure. At 140 °C, the GFPP shows nonlinear behaviour with the strength at failure of approximately 220 MPa at 6% strain. The GFPP matrix is fully melted at 170 °C, leading to textile yarn and undulation straightening under minimum loading up to 2% strain with minimum required load, following by a gradual rise in stress level up to 50 MPa at 3% strain. The

**Fig. 6** **a** Major strain field of steel hourglass shape with 25 mm middle width, **b** major and minor strain graphs versus the section length for the image acquired immediately prior to cracking



stress then continues linearly, increasing up to the failure point at almost 222 MPa and 6.7% strain.

Considering the GFPP material characteristics in the 0/90 fibre orientation, together with the failed test specimens at different temperatures, the GFPP provides relatively high extensibility at 140 °C as well as keeping the composite structure intact. The GFPP at 140 °C has similar strength and close to the same strain at failure limit as those of the GFPP at 170 °C, which suffers from composite matrix melting. Besides, the GFPP strain at failure at 140 °C is more than twice that of the GFPP at room temperature.

The GFPP shear stress-strain graphs at different temperatures are presented in Fig. 9. The shear property of glass fibre reinforced thermoplastic composite was calculated according to ASTM D3518/D3518M-94 [26]. Overall, increasing the temperature leads to decreasing the GFPP shear modulus

and increasing the GFPP shear strain at failure. The GFPP shear strength increases nonlinearly to 24.5 MPa stress at 0.22 shear strain at room temperature, and it plateaus to a failure point at a shear strain of 0.42. The GFPP shear characterization behaviour shows a similar pattern over the range of temperatures 100 to 140 °C, an exponential increase in shear strength, and then a polynomial rise in stress level. The GFPP at 170 °C shows minimum shear strength of 3 MPa at the ultimate failure point.

### Forming tests

The deformed FMLs, pre-heated at 140 °C, are shown in the Fig. 10a. It was found that the FML GFPP layer was drawn into the die and slipped between steel layers without exhibiting any failure (wrinkling, and fibre fracture), and the

**Fig. 7** Tensile engineering stress-strain of steel demonstrated at the rolling, 45°, and transverse directions. Graphs of two samples for each direction are demonstrated and highlighted with the sample number in the figure legend

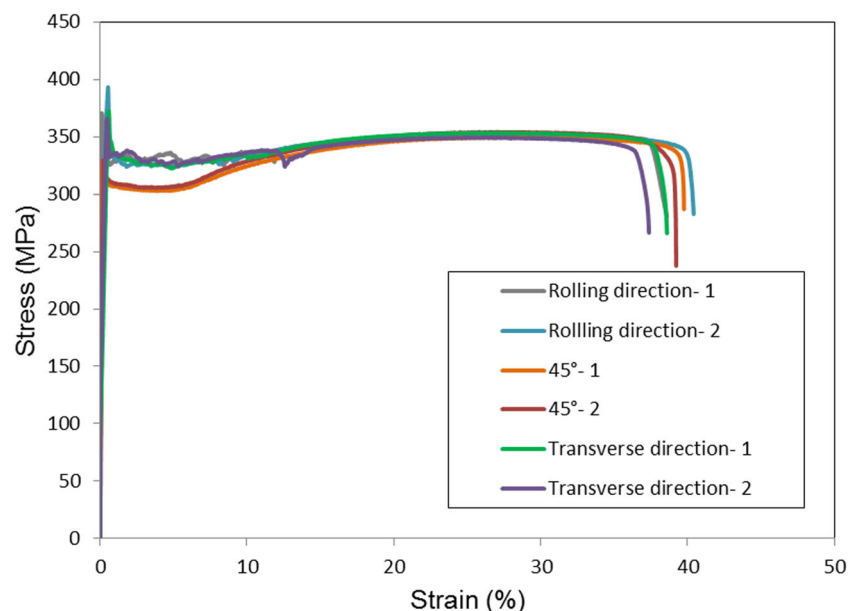
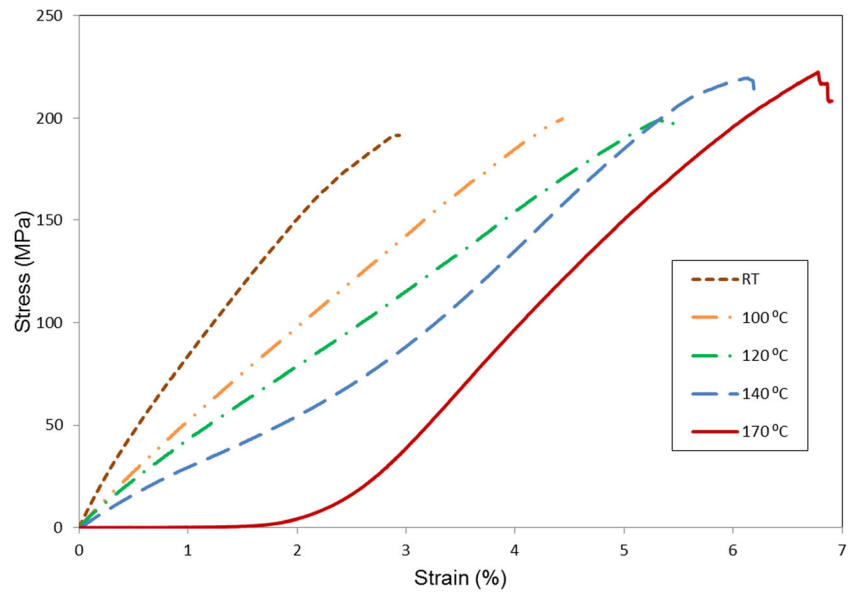


**Fig. 8** Tensile properties of GFPP at different temperatures



FML steel layers were stretched to failure during the forming process. The flow of the polymer matrix minimised stress on the fibres and enabled them to be drawn into the die with the steel.

The deformed FMLs, at 170 °C pre-heat temperature, are shown in Fig. 10b. Visual observation indicates the steel layers were stretched to failure. Since the composite matrix was melted at this temperature, composite thinning and flow of the PP matrix out from the lock ring region was observed. Therefore it is concluded that the flow behaviour of the matrix makes it difficult for the hybrid material configuration to remain intact when forming at 170 °C.

Stretch-formed monolithic steel sheet samples 0.45 mm thick are shown in Fig. 10c. The deformed blanks demonstrated that failure occurred at the desired region according to ISO 12004-2 and no premature failure or blank slippage out of the lock ring was seen during stretch-forming.

**FML forming analysis**

Figure 11 presents FLDs of the steel skin and the FMLs, preheated to 140 and 170 °C, at the principal strains state obtained from the image immediately prior to the bottom steel layer cracking. The strain ratios of the steel formed under the

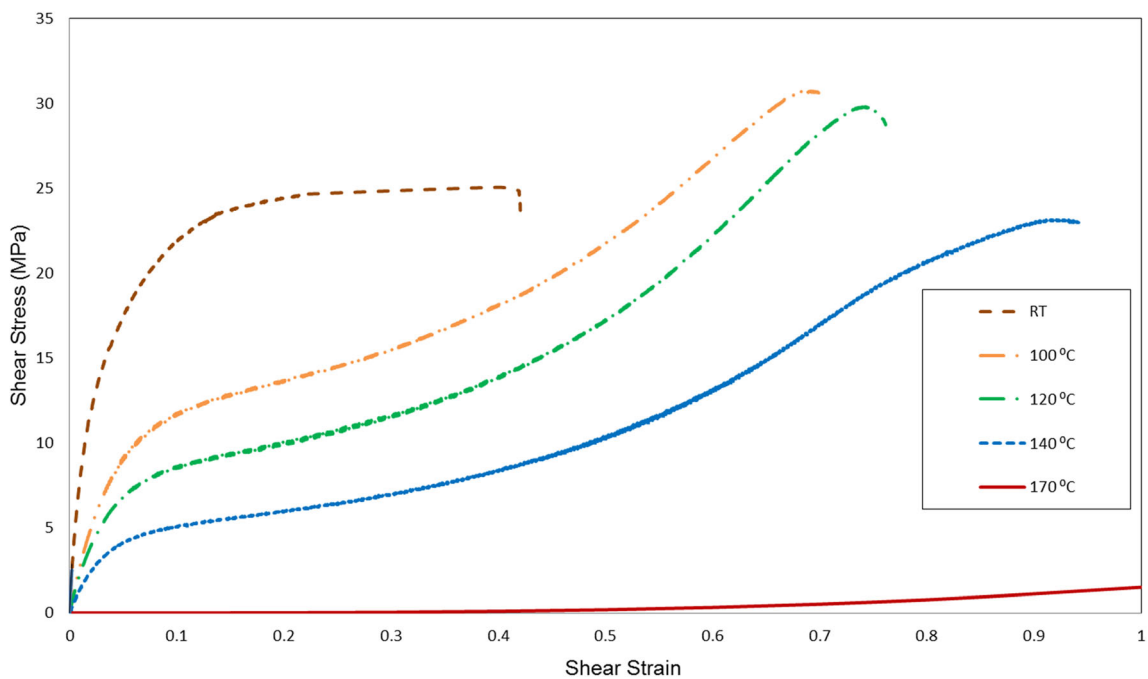


**Fig. 9.** The GFPP engineering shear stress-strain curves at different temperatures

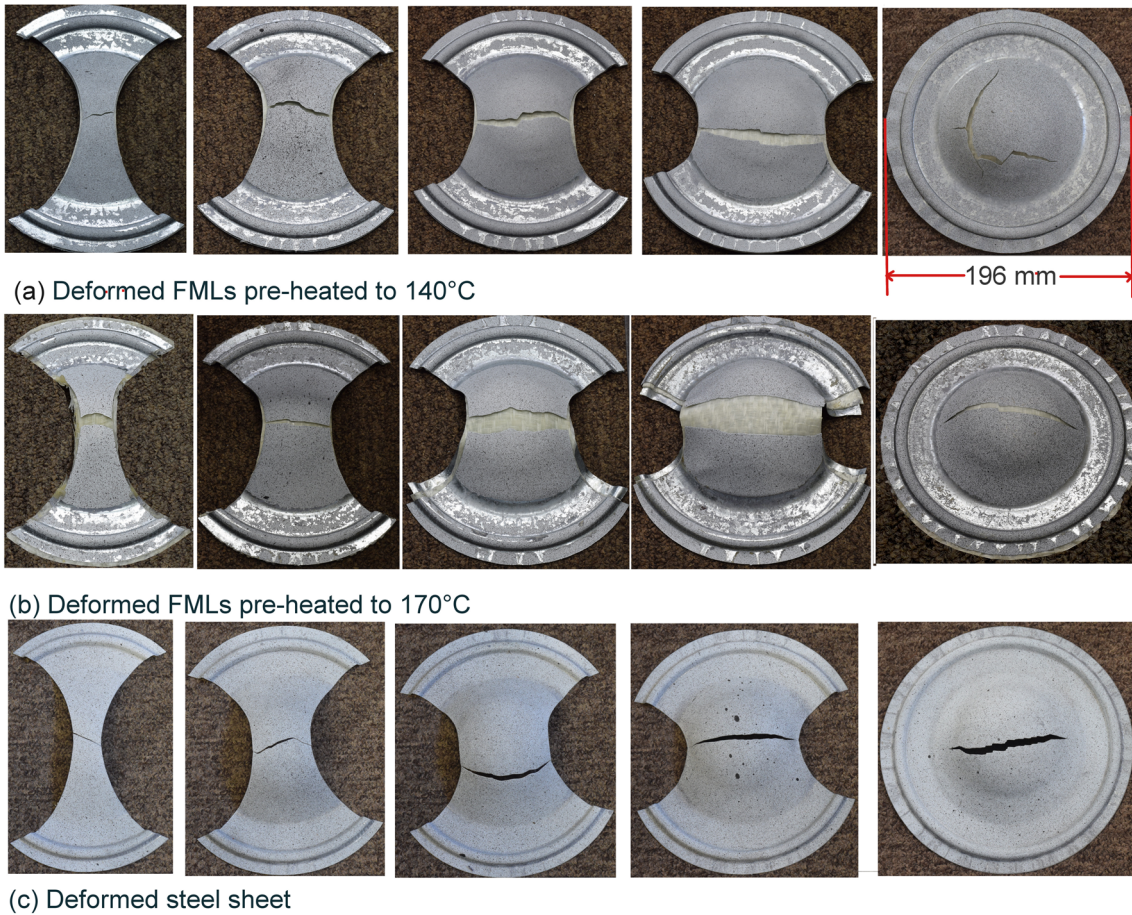


**Fig. 10** Deformed specimens at (a) FMLs pre-heated to 140 °C, (b) FMLs pre-heated to 170 °C, and (c) steel sheet. Deformed blanks from left to right correlate to strain ratio of negative to positive, resulted from

blank geometrical shapes under the stretching condition with the utilization of lubricants for FLC generation

Nakazima test approach covers the in-plane principal strains space. The FLDs of the FMLs show comparable major strains to that of the steel. The obvious difference between the FLDs of FMLs and steel is the deformation mode imposed on the

full circular FML preheated to 140 °C. Although the blank was formed with lubricants between the punch and the blank, the interlayer interactions between the GFPP and the steel layers of FMLs resulted in a slight slippage of the FML layer

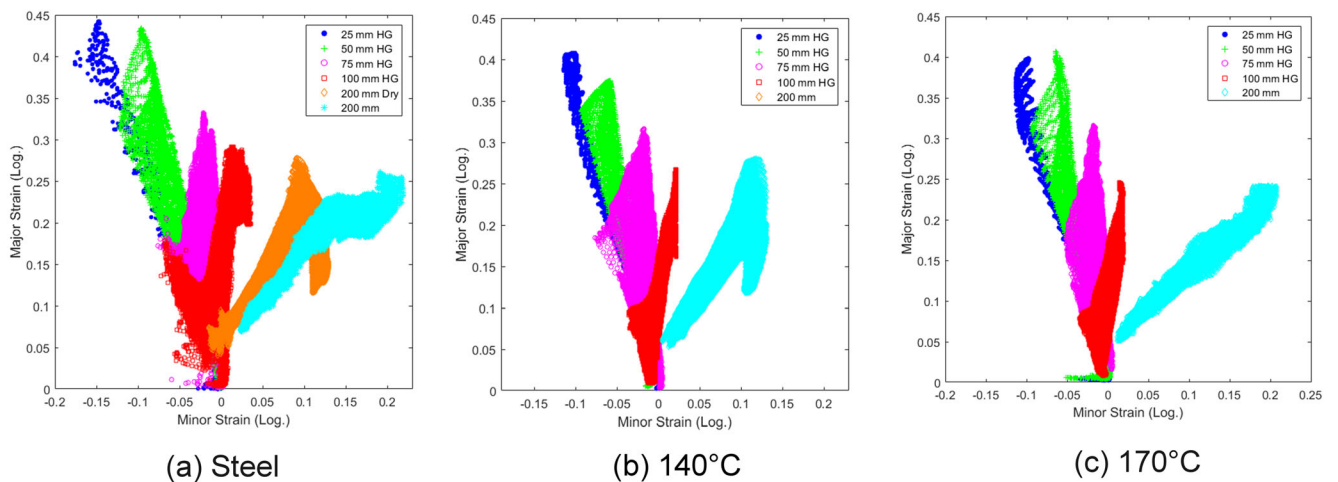


**Fig. 11** Forming limit diagrams (FLDs) obtained from the image immediately prior to the bottom steel layer cracking, measured on the hourglass (HG) and full circular specimens at high temperatures compared with that of the steel skin



and affected the deformation mode imposed on the FML. The deformation mode of the full circular FML, again preheated to 140 °C (marked with cyan in Fig. 11b) is similar to the deformation mode of the full circular steel blank formed without lubricants (marked with orange in Fig. 11a), which demonstrates the occurrence of internal friction between FML layers at 140 °C. Since the deformation mode of the full circular FMLs at 170 °C did not deviate from the deformation mode of its steel counterparts (under the same conditions of stretch and friction), interactions between the FML layers lead the melted composite matrix being squeezed out of the die rather than affecting the deformation mode of the FML bottom steel layer.

The strain path evolutions which were obtained from the points initiated the catastrophic failure, are presented in Fig. 12. For steel, it can be seen that the deformation modes induced on the blanks to failure cover a wider range of minor strain compared to FMLs. FMLs show similar deformation modes on the hourglass shaped specimens at both 140 and 170 °C temperatures. Unlike the full circular FML at 170 °C which experienced an almost biaxial stretch to failure, the full circular FML at 140 °C exhibited a deformation mode between plane strain and biaxial stretching modes, similar to the deformation mode of steel stretch-formed under dry condition.

### Forming limit curves (FLCs)

FLCs of the steel and FMLs are shown in Fig. 13. The FLC of FMLs is dominated by the bottom steel forming limits, considering the interlayer slippage between the GFPP and steel layers. Both FMLs have comparable formability to the steel however the FMLs pre-heated to 140 °C remained intact during the forming process, that is, no composite or fibre failure was observed, due to the composite interlayer slippage.

Considering the fact that bonding between FML layers weakened at a higher temperature and the load transfer mechanism between the layers changed to friction-based contact, the GFPP slipped through the steel layers into the die. On the other hand, forming FMLs at 170 °C resulted in composite thinning and flow of the matrix out of the die.

To investigate the development of the surface strain field over the blanks prior to FML forming limit curve, two hourglass shaped FMLs with middle widths of 50 and 150 mm were selected and preheated to 140 °C, and then formed up to 22 mm before the FML failure depth at this temperature. The surface strain fields for these samples remain within the region, shown in Fig. 5.

### Finite element simulation

Finite element analysis (FEA) is a useful tool in predicting strain states at stamp forming process, and consequently evaluating design with incorporating FLC into the finite element code. In this study, LSDYNA commercial FE software with explicit time step was utilised to simulate the forming process of circular FML, pre-heated to 140 and 170 °C, (Fig. 14). FMLs are simulated with three individual layers, discretising using thin shell elements with 1 mm element size, Belytschko–Leviathan element formulation. The three layers were in contact based on a penalty method. The punch, blank holder, and die were simulated with a rigid material.

Cousigné et al. [26] developed a nonlinear material model for woven composites based on the material constitutive model shown in Eq. (2). Material nonlinearity was simulated based on Ramberg–Osgood equation [27] and user-defined load curve of experimental stress–strain material curves. Wang et al. [28, 29] simulated the stretch forming process of woven flax fibre reinforced polypropylene with a nonlinear

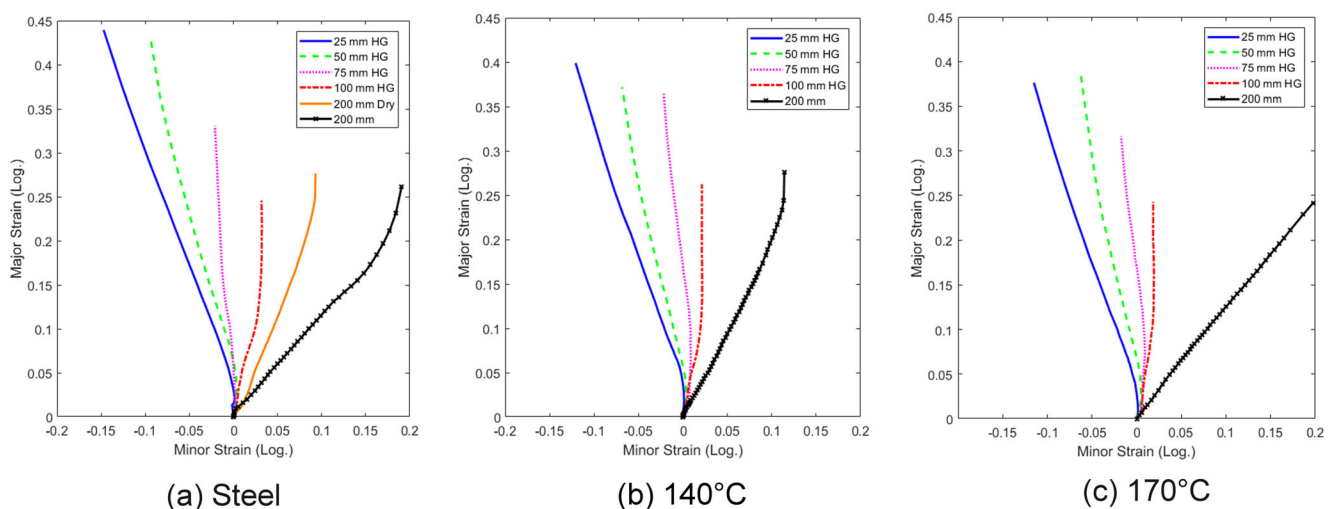
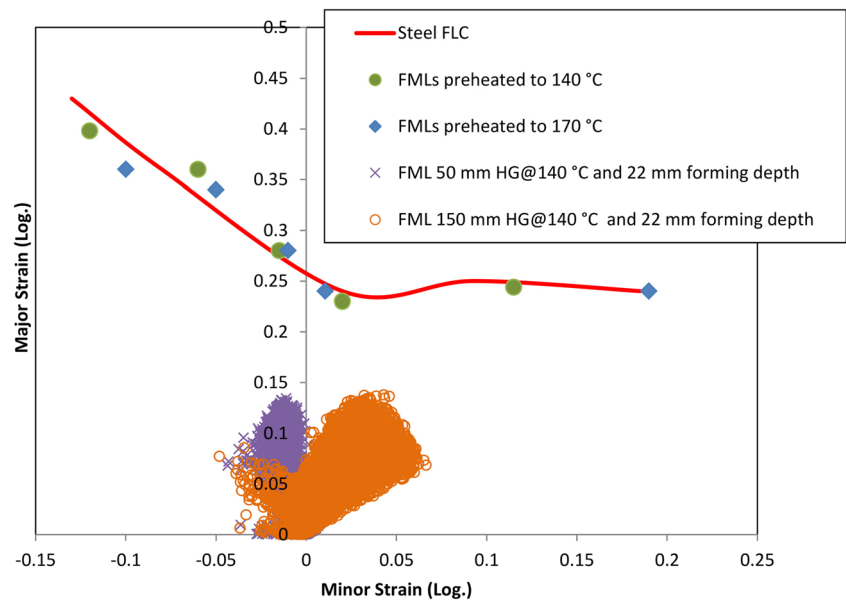


**Fig. 12** The major strain evolution of a point experiencing failure at the final stage of the forming process for different geometrical specimens

**Fig. 13** Forming limit diagram of FMLs, at 140 °C formed up to 22 mm depth, in comparison to FLCs



orthotropic material modelling developed based on Eq. (2). Here, the GFPP orthotropic material model is developed based on the stress-strain relation shown in Eq. (2). This nonlinear numerical model is developed with a user-defined subroutine (UMAT) and incorporated into the FE model.

$$\begin{bmatrix} \sigma_{11} \\ \sigma_{22} \\ \sigma_{33} \\ \tau_{23} \\ \tau_{13} \\ \tau_{12} \end{bmatrix} = \begin{bmatrix} C_{11} & C_{12} & C_{13} & 0 & 0 & 0 \\ C_{12} & C_{22} & C_{23} & 0 & 0 & 0 \\ C_{13} & C_{23} & C_{33} & 0 & 0 & 0 \\ 0 & 0 & 0 & C_{44} & 0 & 0 \\ 0 & 0 & 0 & 0 & C_{55} & 0 \\ 0 & 0 & 0 & 0 & 0 & C_{66} \end{bmatrix} \times \begin{bmatrix} \epsilon_{11} \\ \epsilon_{22} \\ \epsilon_{33} \\ \gamma_{23} \\ \gamma_{13} \\ \gamma_{12} \end{bmatrix} \quad (2)$$

Here,  $C_{11}$ ,  $C_{22}$ ,  $C_{12}$  are calculated from Eqs (3) and (4).  $C_{66}$  is the in-plane shear stiffness. The transverse shear stiffness coefficients,  $C_{44}$  and  $C_{55}$ , are equal to five-sixths of the in-plane shear stiffness [30]. The two-dimensional stress states are calculated using thin shell element type and a plane stress assumption. Then, the rest of the stiffness matrix terms are equal to zero.

$$C_{11} = \frac{E_1}{1-\nu^2} \quad (3)$$

$$C_{22} = \frac{E_2}{1-\nu^2} \quad (4)$$

$$C_{12} = \frac{E_1 \times \nu}{1-\nu^2} \quad (5)$$

$$C_{66} = G_{12} \quad (6)$$

$$C_{44} = C_{55} = \frac{5}{6} C_{66} \quad (7)$$

Here,  $E_1$  and  $E_2$  are the Young’s moduli along principal composite axes,  $G_{12}$  is in-plane shear stiffness and  $\nu$  is the in-plane Poisson’s ratio.

Stress states are incrementally computed and accumulated according to Eq. 8. At each time-step, the stiffness matrix is updated based on current strains, results from accumulating incremental strains, and the material characterization curves. Then, the current stress states are calculated based on the previous stress states, incremental strains, and the updated stiffness matrix.

$$\sigma_i^n = \sigma_i^{n-1} + C_{ij} d\epsilon_j \quad (8)$$

Instantaneous stiffness parameters,  $E_1$ ,  $E_2$  and  $G_{12}$ , are acquired from the derivative of the curves fitted from material characterization graphs in Fig. 7 and Fig. 8 in regard to current strain states and temperature. One of the UMAT subroutine inputs is incremental strains from which the current strain is accumulatively calculated through simulation increments. Finally, Stiffness parameters are calculated based on the interpolation of the stiffness values at the two upper and lower material characterization test temperatures in regard to the instantaneous element temperature and current strain.

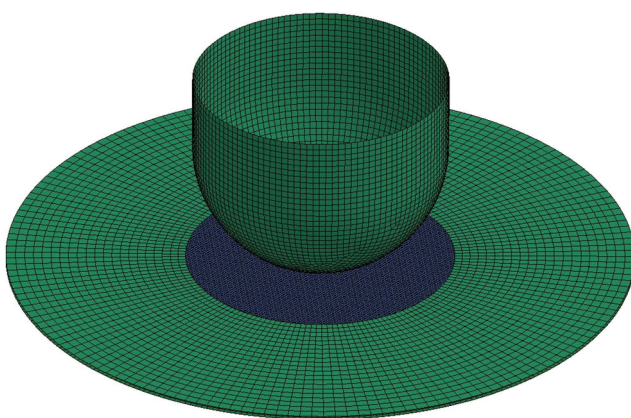


**Fig. 14** The FE model of a circular FML blank with 200 mm diameter

The steel material modelling is developed based on a piece-wise linear plasticity built-in material model from the average graph of the steel material behaviours at different directions shown in Fig. 7. Directionality was just seen between the incipient of the plastic region up to 13% of engineering strain, limited to a small region of total steel strain of 40%. So, simulating the steel with piece-wise linear plasticity numerically provides reasonable material behaviour during stretch forming and especially at the steel forming limits.

The isotropic thermal modelling from LSDYNA built-in material library and one way thermal-mechanical coupling explicit solver were used for including the heat transfer between material layers and press setup during forming. The composite at 140 °C did not experience failure including thinning or composite matrix flowing out after forming and therefore, the increase of temperature due to external work was considered.

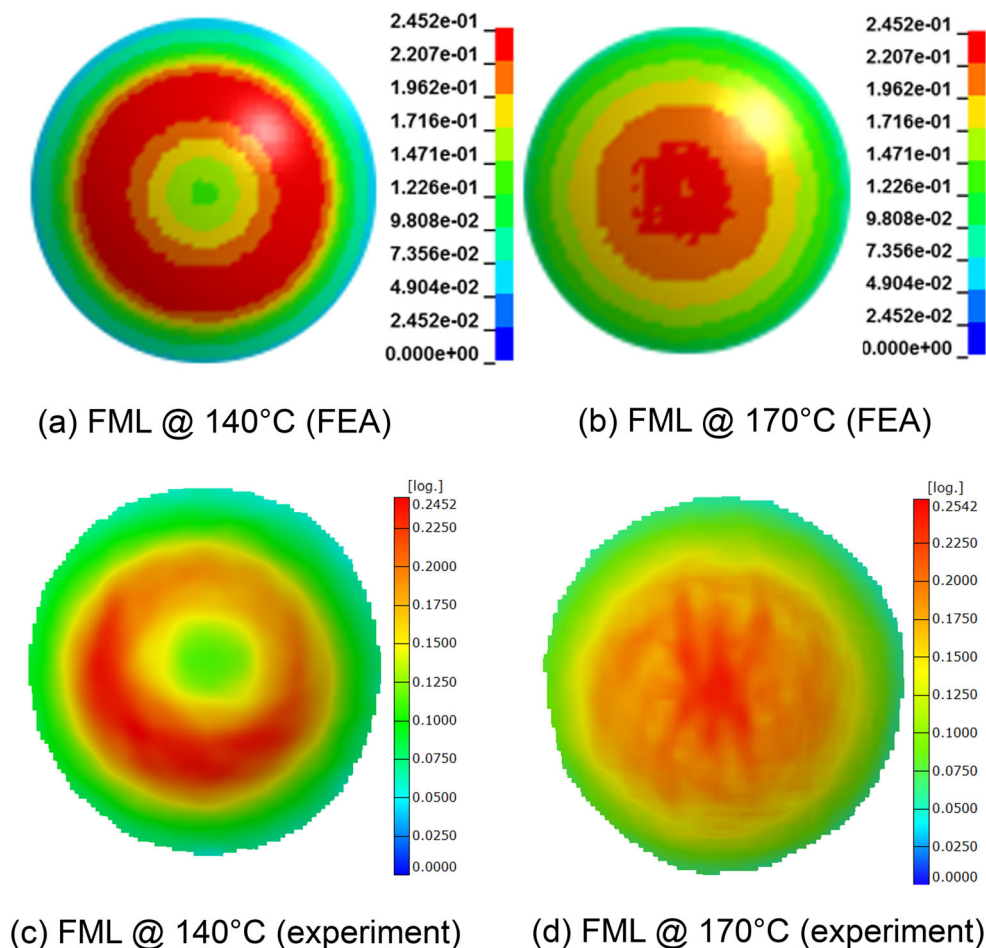
The numerical and experimental major strain fields over the bottom surface of FMLs, pre-heated to 140 and 170 °C, at the onset of necking are compared in Fig. 15, demonstrating a reasonable agreement between experiments with numerical results. In Fig. 15d, the experimental result shows FML strain band, preheated at 170 °C, which was under the effect of glass

fibre yarns stretching due to matrix melting down and had a vertical trace. The FML at 170 °C experienced failure at a region near pole (centre of the sample), whereas the FML at 140 °C experienced higher strain at a region away from the pole, which led to failure in that region.

### Conclusions

Fibre metal laminates (FMLs) comprised of 0.45 mm thick sheet steel and a 0/90 twill weave fibre-glass reinforced polypropylene (GFPP) with 1 mm thickness were manufactured in a 2:1 configuration. They were preheated to 140 and 170 °C then stretch formed using a hemi-spherical punch. The monolithic sheet steel (0.45 mm thick) was also stretch formed. Forming was undertaken using an open die to enable measurement of the strain field on the bottom steel layer using a real-time 3D measurement system (ARAMIS) during the forming process. The forming limit curves (FLCs) of the steel and FMLs were established based on ISO 12004-2. The FLC of FMLs demonstrated forming limits comparable to that of the steel skin. The GFPP composite layer of the FMLs pre-heated to 140 °C remained intact and was pulled into the die

**Fig. 15** Major strain fields over full circular blanks formed under the stretching condition with the utilization of lubricants are measured by ARAMIS (experimental results) and FEA results



alongside with steel layers being stretched due to interlayer slippage. The FML pre-heated to 170 °C (the composite matrix melt temperature) exhibited composite thinning and flow of the matrix out of the die. Therefore, pre-heating pre-consolidated FMLs to 140 °C increases FMLs formability similar to the monolithic steel. Pre-heating FMLs to 140 °C causes the composite matrix to be softened and also FML bonding layers are melted down, providing an opportunity for the GFPP middle layer to be drawn into the die. Through curve-fitting technique of composite material characterization test results, the GFPP numerical model was developed with the UMAT. The FE simulation demonstrated a good agreement with the experiments, resulting to examining the application of this process for parts production from FML pre-consolidated panels in regard to the material FLC.

**Acknowledgements** This research is supported by an Australian Government Research Training Program (RTP) Scholarship.

### Compliance with ethical standards

**Conflict of interest** The authors declare that they have no conflict of interest.

### References

- Reyes G, Cantwell WJ (2000) The mechanical properties of fiber-metal laminates based on a glass fibre reinforced polypropylene. *Composites science and technology* 9(7):211–216. [https://doi.org/10.1016/S0266-3538\(00\)00002-6](https://doi.org/10.1016/S0266-3538(00)00002-6)
- Reyes G, Kang H (2007) Mechanical behavior of lightweight thermoplastic fiber-metal laminates. *J Mater Process Technol* 186(1-3): 284–290. <https://doi.org/10.1016/j.jmatprotec.2006.12.050>
- Vogelings LB, Vlot A (2000) Development of fibre metal laminates for advanced aerospace structures. *J Mater Process Technol* 103(1). [https://doi.org/10.1016/S0924-0136\(00\)00411-8](https://doi.org/10.1016/S0924-0136(00)00411-8)
- Compston P, Cantwell WJ, Jones C, Jones N (2001) Impact perforation resistance and fracture mechanisms of a thermoplastic based fiber-metal laminate. *J Mater Sci Lett* 20(7). <https://doi.org/10.1023/A:1010904930497>
- Botelho EC, Silva RA, Pardini LC, Rezende MC (2006) A review on the development and properties of continuous Fiber / epoxy / aluminum hybrid composites for aircraft structures. *Mater Res* 9(3). <https://doi.org/10.1590/S1516-14392006000300002>
- Keeler S, Backhofen W (1964) Plastic instability and fracture in sheet stretched over rigid punches. *ASM Transactions Quarterly* 56:25–48
- Nakazima, K., Kikuma, T., Hasuka K (1968) Study on the formability of steel sheets. Technical Report Yawata Technical Report
- Marciniak Z, Kuczyński K (1967) Limit strains in the processes of stretch-forming sheet metal. *Int J Mech Sci* 9(9):609–620. [https://doi.org/10.1016/0020-7403\(67\)90066-5](https://doi.org/10.1016/0020-7403(67)90066-5)
- ISO/DIS 12004–2 (2008) Metallic Materials - Sheet and Strip - Determination of Forming Limit Curves - Part 2: Determination of Forming Limit Curves in the Laboratory. International Organization for Standardization 20087. 2:12004
- Sokolova O, Carradó A, Palkowski H (2010) Production of customized high-strength hybrid Sandwich structures. *Adv Mater Res* 137:81–128. <https://doi.org/10.4028/www.scientific.net/AMR.137.81>
- Mosse L, Compston P, Cantwell WJ, Cardew-Hall M, Kalyanasundaram S (2006) Stamp forming of polypropylene based fibre-metal laminates: the effect of process variables on formability. *J Mater Process Technol* 172(2):163–168. <https://doi.org/10.1016/j.jmatprotec.2005.09.002>
- Mosse L, Compston P, Cantwell WJ, Cardew-Hall M, Kalyanasundaram S (2006) The development of a finite element model for simulating the stamp forming of fibre-metal laminates. *Compos Struct* 75(1-4):298–304. <https://doi.org/10.1016/j.compstruct.2006.04.009>
- Gresham J, Cantwell W, Cardew-Hall MJ, Compston P, Kalyanasundaram S (2006) Drawing behaviour of metal-composite sandwich structures. *Compos Struct* 75(1-4):305–312. <https://doi.org/10.1016/j.compstruct.2006.04.010>
- Mosse L, Compston P, Cantwell WJ et al (2005) The effect of process temperature on the formability of polypropylene based fibre-metal laminates. In: *composites part a: applied science and manufacturing*, pp 1158–1166
- Compston P, Cantwell WJ, Cardew-Hall MJ, Kalyanasundaram S, Mosse L (2004) Comparison of surface strain for stamp formed aluminum and an aluminum-polypropylene laminate. *J Mater Sci* 39(19):6087–6088. <https://doi.org/10.1023/B:JMSC.0000041707.68685.72>
- Sexton A, Cantwell W, Kalyanasundaram S (2012) Stretch forming studies on a fibre metal laminate based on a self-reinforcing polypropylene composite. *Compos Struct* 94(2):431–437. <https://doi.org/10.1016/j.compstruct.2011.08.004>
- Rajabi A, Kadkhodayan M, Manoochehri M, Farjadfar R (2015) Deep-drawing of thermoplastic metal-composite structures: experimental investigations, statistical analyses and finite element modeling. *J Mater Process Technol* 215. <https://doi.org/10.1016/j.jmatprotec.2014.08.012>
- Wollmann T, Hahn M, Wiedemann S, Zeiser A, Jaschinski J, Modler N, Ben Khalifa N, Meißer F, Paul C (2018) Thermoplastic fibre metal laminates: stiffness properties and forming behaviour by means of deep drawing. *Archives of Civil and Mechanical Engineering* 18(2). <https://doi.org/10.1016/j.acme.2017.09.001>
- Jalali Aghchai A, Khatami S (2018) Experimental and numerical formability investigation of FML sheets with glass fiber reinforced core. *Int J Adv Manuf Technol* 96:9–12. <https://doi.org/10.1007/s00170-018-1836-x>
- Zhu B, Yu TX, Tao XM (2009) Large shear deformation of E-glass/polypropylene woven fabric composites at elevated temperatures. *J Reinf Plast Compos* 28(21):2615–2630. <https://doi.org/10.1177/0731684408093095>
- Hou M, Friedrich K (1994) 3-D stamp forming of thermoplastic matrix composites. *Appl Compos Mater* 1(2):135–153. <https://doi.org/10.1007/BF00567575>
- MacHado M, Murenu L, Fischlschweiger M, Major Z (2016) Analysis of the thermomechanical shear behaviour of woven-reinforced thermoplastic-matrix composites during forming. *Compos A: Appl Sci Manuf* 86:39–48. <https://doi.org/10.1016/j.compositesa.2016.03.032>
- Tepex® Dynalite (2014) Material Data Sheet. [http://bond-laminates.com/uploads/tx\\_txsmatrix/600:7072](http://bond-laminates.com/uploads/tx_txsmatrix/600:7072)
- ARAMIS (2009) ARAMIS user manual
- Marciniak Z, Duncan J, Hu SJ (2002) Mechanics of sheet metal forming
- D 3518 (2007) Standard test method for in-plane shear response of polymer matrix composite materials by tensile test of a +45 ° laminate. *Annual Book of ASTM Standards* <https://doi.org/10.1520/D3518>

28. Bogetti TA, Hoppel CPR, Harik VM et al (2004) Predicting the nonlinear response and progressive failure of composite laminates. Failure Criteria in Fibre-Reinforced-Polymer Composites 64:402–428. <https://doi.org/10.1016/B978-008044475-8/50017-2>
29. Wang W, Lowe A, Kalyanasundaram S (2016) Investigating the forming limits of a flax fibre-reinforced polypropylene composite in different water treatment conditions. International journal of advanced manufacturing technology 1–11
30. Wang W, Lowe A, Davey S, Akhavan Zanjani N, Kalyanasundaram S (2015) Establishing a new forming limit curve for a flax fibre reinforced polypropylene composite through stretch forming experiments. Compos A: Appl Sci Manuf 77:114–123. <https://doi.org/10.1016/j.compositesa.2015.06.021>
31. Ls-dyna, software LS, Orporation TEC (2017) Theory Manual 01/26/18

**Publisher's note** Springer Nature remains neutral with regard to jurisdictional claims in published maps and institutional affiliations.